Proceedings World Geothermal Congress 2020+1
Reykjavik, Iceland, April - October 2021

Numerically Stable Computation of the Thermodynamics Properties of Water using Splines

Martin Letourneur[1], David Dempsey[1], John O'Sullivan[1], Mike O'Sullivan[1], Adrian Croucher[1]

[1]Department of Engineering Science, University of Auckland, Auckland, New Zealand

martin.letourn@gmail.com

Keywords: water, thermodynamics, pressure, enthalpy, density, viscosity, temperature, splines, continuous, derivatives, flow, simulation

ABSTRACT

In geothermal modelling, a stable method for computing the thermodynamic properties of water – density, temperature and viscosity – is essential. Instability can lead to convergence issues within the flow simulator. For water, the most common way of computing those properties is through using either Gibbs or Helmholtz equations depending on the pressure (p) and enthalpy (h) region the fluid is in. However, the boundaries between the different regions present some discontinuities in the values of fluid properties, which can cause slow convergence of the flow simulator. In the past, these discontinuities have been addressed through the introduction of blending zones between regions to ensure a smooth transition.

Our work aims to implement an efficient method of computing fluid properties that builds in property and derivative continuity across the entire p-h domain. We do this by using bivariate splines with optimised, non-uniform knot locations. In addition to increased stability of the computation, this grants easy access to the derivatives of fluid properties with respect to pressure and enthalpy. This is important for some methods of reservoir simulation and optimization.

The methodology presented in this paper is as follows. First, we assemble data related to the water properties we are interested in. Second, we introduce an algorithm capable of building a bivariate spline approximation that captures the complexity of our datasets while remaining sufficiently smooth. Third, we perform a quality check on the relative errors, partial derivatives and continuity of our surfaces. Finally, we implement our thermodynamic formulation into a flow simulator in order to assess its performance and precision.

1. INTRODUCTION

An important component of any flow simulation software is the formulation of the thermodynamics properties. In our paper, we take interest in the formulation of the properties of water. The most common formulations are the IFP-67 (IAPWS, 2007) and the IAPWS (IAPWS, 2018) which divide the domain into five thermodynamic regions (Figure 1). Each region has its own equation that computes the various properties. Such formulations have proven precise and efficient in most cases but they do have some flaws. The first is the existence of discontinuities at the boundary between two regions (O'Sullivan, 2016),which can cause convergence problems in a flow simulation. The second is that such formulations do not offer easy access to the partial derivatives of the fluid properties.

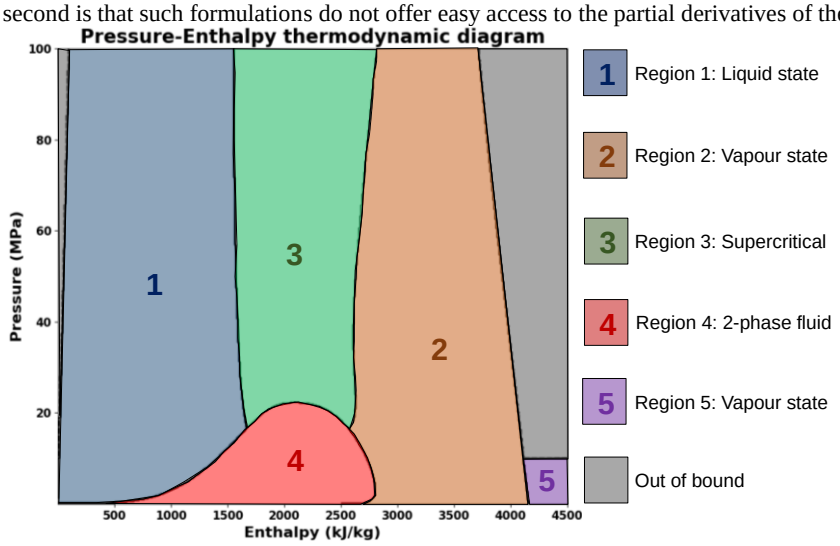

Figure 1: Pressure-enthalpy diagram showing the different thermodynamic regions for pure water

In an effort to prioritize continuity and differentiability of fluid properties across the domain, we have developed a new formulation based on the bivariate splines approximation. The IAPWS have published a bivariate spline based formulation (IAPWS, 2015), however, as there is a different set of splines for each thermodynamic region, this does not resolve the problem of interface discontinuities. In the past, these discontinuities have been addressed through the introduction of blending zones that ensure a smooth transition between regions (Åberg, 2017; O'Sullivan, 2016). Here, we use a single set of bivariate splines for the entire single phase thermodynamic domain (i.e., regions 1,2,3 and 5).

2. METHODS IMPLEMENTED

2.1. Data acquisition

In order to build our spline approximation, we require reliable information about the properties of water. We have elected to use the IAPWS formulation (IAPWS, 2018) as it is the most recognized. This formulation uses different equations depending on the thermodynamic region. For pure liquid and pure vapour, the formulation uses the Gibbs equation, which depends on pressure and temperature. For the supercritical region, the formulation uses the Helmholtz equation, which depends on density and temperature. Inverse relationships exist in order to express density, viscosity and temperature with respect to pressure and enthalpy. Modelica (Jain, 2017) implements these thermodynamics relationship in their open source library. In order to build our dataset, we first translated the Modelica formulation into Python.

The dataset is structured as a regular grid of resolution 100×100 for enthalpies between 1 and 4500 kJ kg^{-1} and pressures between 611.657 Pa and 100 MPa. With the rectangular geometry, some of data points fall out of bounds as the thermodynamic regions themselves are not rectangular (Figure 1). We use bilinear interpolation to estimate parameters values in the out of bound regions so that we can obtain the smoothest dataset possible. We also populate the two-phase region using the formulation described in the IAPWS formulation (IAPWS, 2018).We chose not to extend our formulation to the two-phase region as its boundary presents a discontinuity in terms of derivatives that is physically relevant and should not be smoothed by a bivariate spline approximation. The thermodynamic parameters in the two phase region can be expressed by coupling the splines formulation with the IAPWS relationships. From the previous spline approximation of the thermodynamics of water (Åberg, 2017; IAPWS, 2015), we set our maximum acceptable margin of error at 1%.

2.2. Bivariate splines approximation principle

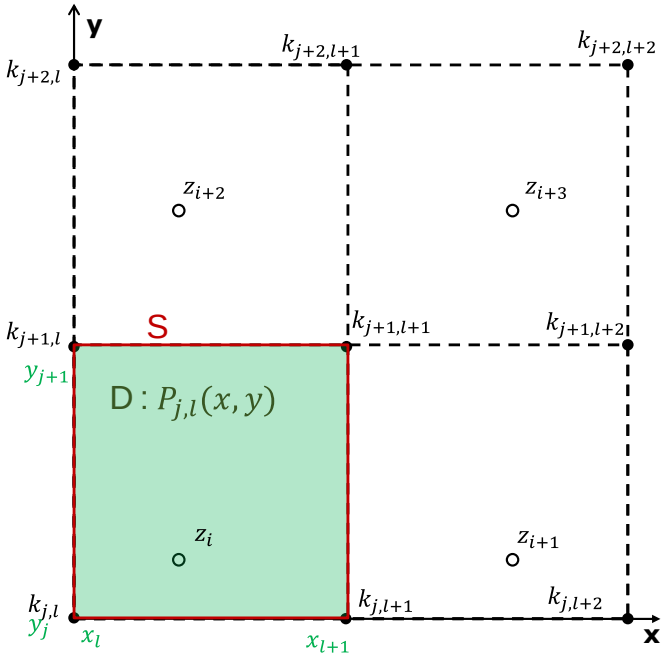

Figure 2: Schematic showing the principle of bivariate spline approximation. The open circles represent the dataset, z_i, to be fitted. The dotted lines represent the boundary of each subdomains delimited by four knots each (filled circles). On each subdomain, a single polynomial function is defined.

Consider a data set comprising d^2 sampling points taken on a uniform grid of dimension $d \times d$ (Figure 2). The data set represent measurement of a field z with respect to x and y coordinates. Each sampling point has its own set of coordinates $[xi, yi, zi]$. The domain of the approximation is $[min(x), max(x)] \times [min(y), max(y)]$. The principle of the bivariate splines approximation is to build a piecewise function spl consisting of $m \times n$ polynomial functions. Each polynomial function is defined on a given rectangular subdomain D: $[x_l, x_{l+1}] \times [y_j, y_{j+1}]_{l \in [\![1,m-1]\!], j \in [\![1,n-1]\!]}$. The set of coordinates defining the subdomain boundaries are called the knots.

On a given subdomain, the optimal coefficients of the polynomial function $P_{j,l}$ are found by minimising the sum of squares residual $\sum_1^k (z_i - P_{j,l}(x_i, y_i))^2$, where k is the number of data points that are part of the subdomain. The polynomial functions are also subject to additional boundary conditions that ensure the resulting function spl is continuous in value and derivative at subinterval boundaries. If two polynomial functions P, Q defined on neighboring subdomains sharing an interface S, then the boundary condition can be expressed as $\begin{cases} P(x_s, y_s) = Q(x_s, y_s) \\ P'(x_s, y_s) = Q'(x_s, y_s) \end{cases}, (x_s, y_s) \in S$ where the prime indicates a derivative in x or y directions. Furthermore, we can apply different weights on the samples forming the dataset. This provides more control over which features of the dataset we want to capture most accurately. In this case, we minimize the weighted sum of squared residual $\sum_1^k (w_i(z_i - P_{j,l}(x_i, y_i)))^2$ to find the optimal polynomial coefficients, where $w_i$is the weight of the data point z_i. Numerically, the function spl can be defined by its knots on both x and y axis, its polynomial coefficients and the order of the polynomials. In our work we used the Python class scipy.interpolate.LSQBivariate to solve the system of equation for a given set of data points, knots, weights and polynomial orders.

2.3. Knot position optimization

The quality of a bivariate splines approximation depends greatly on the distribution of knots. A simple 2D case is shown in Figure 3. If the number of knots is too low then the approximation won't capture the whole complexity of the data (Figure 3B). If the number of knots is too high then the resulting function will perfectly match all sampling point but will also present steep gradients between adjacent data points (Figure 3A).

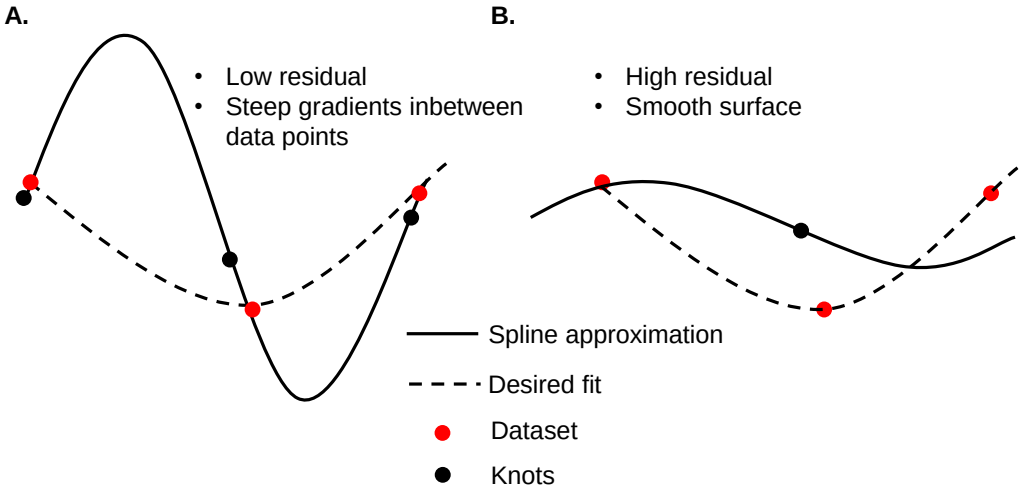

Figure 3: A. Schematic showing a simple case of over fitting. B. Schematic showing a simple case of under fitting.

Since we are fitting thermodynamic properties, the function we are seeking needs to capture data complexity while also remaining as smooth as possible. Furthermore, the more knots we use, the slower the execution time of the thermodynamic routines. Therefore, both the number and the position of the knots need to be optimised. Our optimization process is described in Figure 4, similar algorithms have already been presented in further detail (Schütze, 2001).

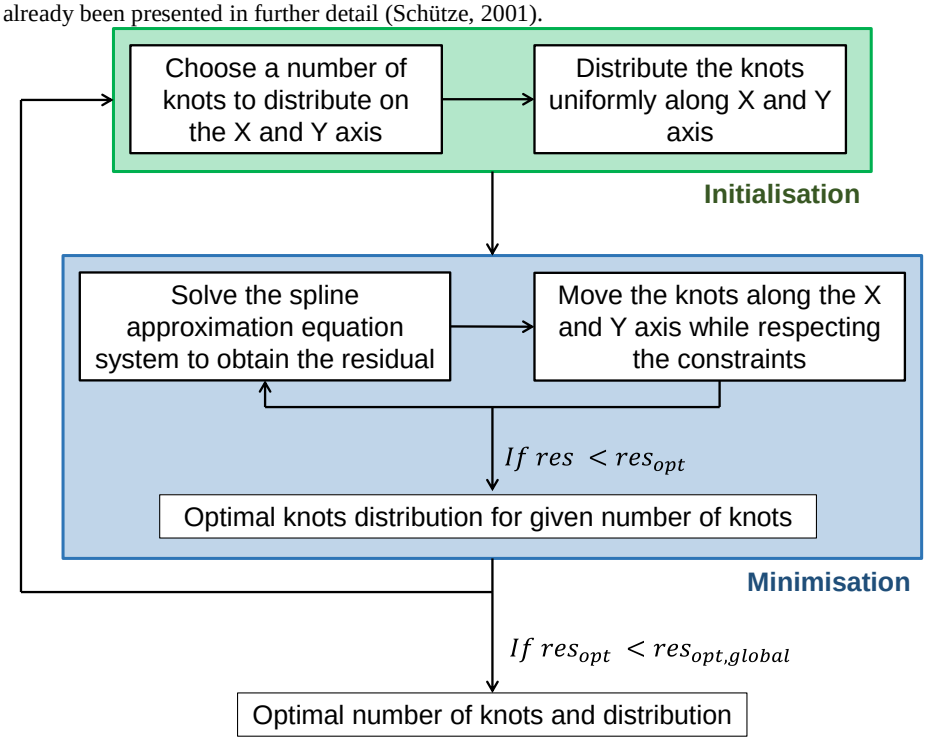

Figure 4: General flow chart of the knot optimization process.

In our case the convergence criteria is a tolerance on the variation of the residual between two iterations. The minimization is handled by the Python function scipy.optimize.minimize using the sequential least squares programming method. The result of such optimization is a distribution in which complex areas of the domain have a higher concentration of knots than smoother areas.

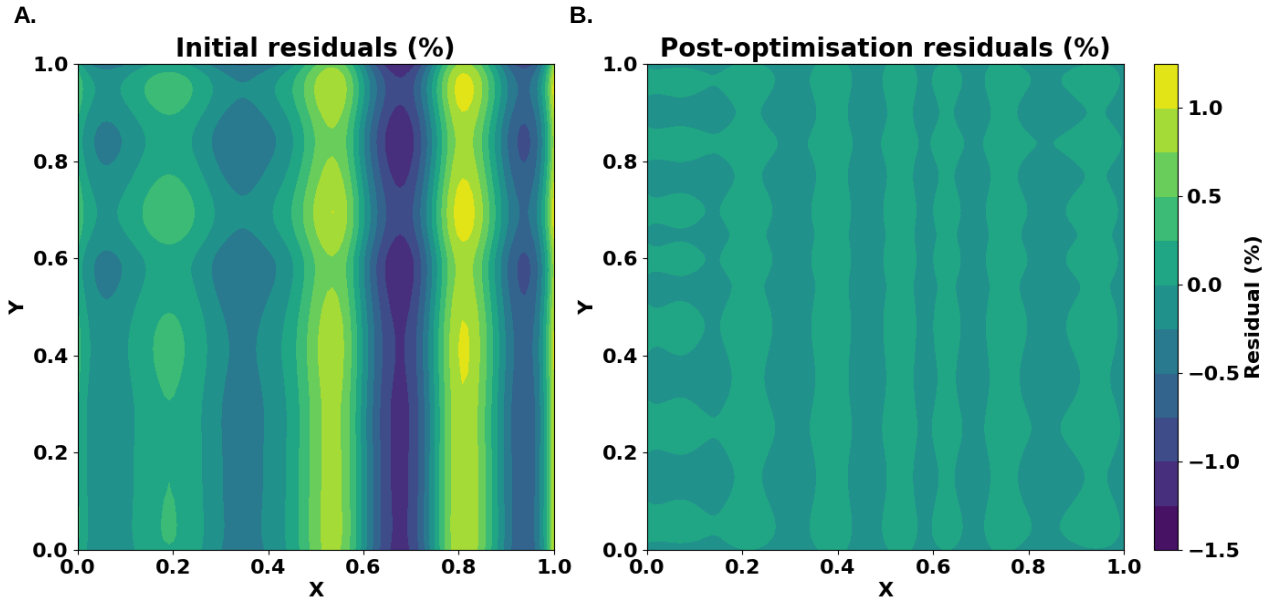

Figure 5: Contour plots showing the residual between the dataset and the spline approximation. A. Initial state. B. Final state after running our optimization algorithm.

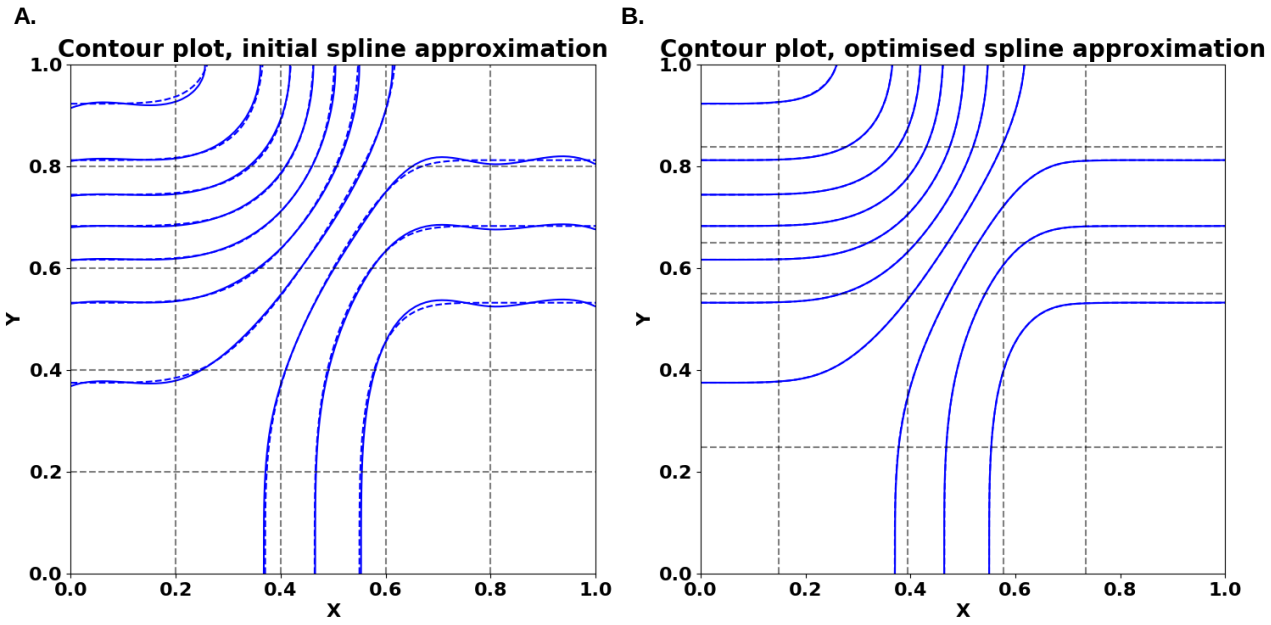

Figure 6: Contour plots showing the knot distribution (dashed grey lines), dataset (dashed blue lines) and the spline approximation (blue lines). A. Initial state. B. Final state after running our optimization algorithm.

An example of knot optimization is given in Figure 5 and Figure 6. In the initial state, the knots are uniformly distributed throughout the domain. In that configuration, the right-hand side of the domain ($x > 0.5$) displays the highest residuals and the contours of the original surface can be distinguished from the spline approximation0 (Figure 5A and Figure 6A). After optimization, the knot distribution is no longer uniform. The central part of the domain concentrates a finer grid of knots than the rest of the domain (Figure 6B) and the residual has been substantially reduced throughout (Figure 5B).

2.4. Weight distribution optimization

Fitting a dataset using splines has its constraints. A polynomial function is relatively smooth and has no vertical asymptotic behavior. Therefore it can be difficult to capture steep gradients in the dataset such as exist in the thermodynamic properties of water. In Figure 7 and Figure 8, we display an example of such behavior with a dataset containing steep regions. When using a uniform weight distribution, the final knot position is almost equal to the initial uniform knot distribution and we are left with large residuals in the steep regions (Figure 7A and Figure 8A). The knot optimization performs poorly because each residual in the dataset has the same impact on the global system residual. To obtain a better fit in steep regions, the algorithm compensates by decreasing the residual in smooth regions. In order to counter this behavior, we use a modified weight distribution to amplify the impact of the residuals in steep regions. Then, the algorithm won't be able to compensate the large residuals and it will be forced to find a better fit. In that case the weight of a point is given by $w = a \times \max(grad_x, grad_y) + b$, where a, b are some constants.

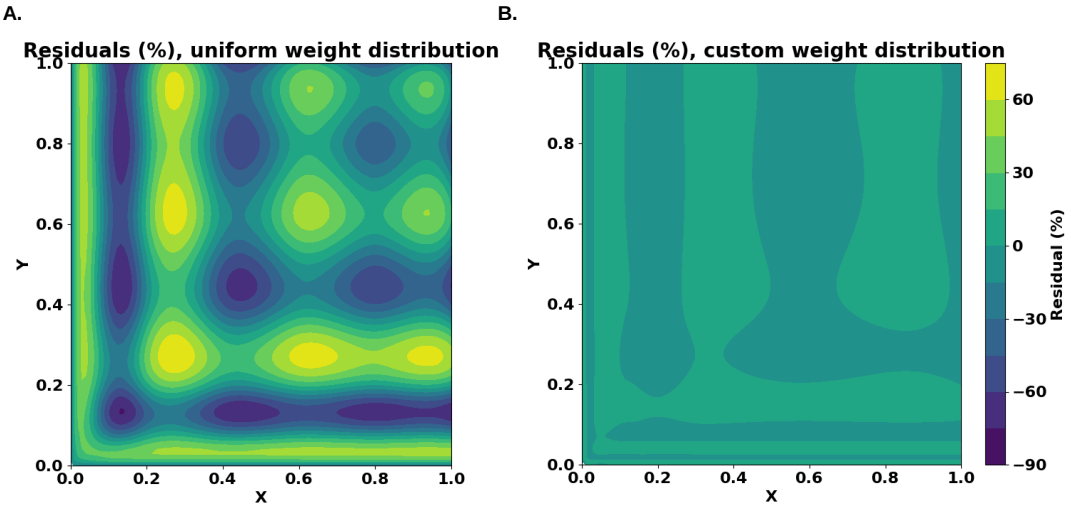

Figure 7: Contour plots showing the residuals between the dataset and the spline using different weight distributions. A. Using a uniform weight distribution. B. Using a custom weight distribution. Both plots are obtained after running our knots optimization algorithm

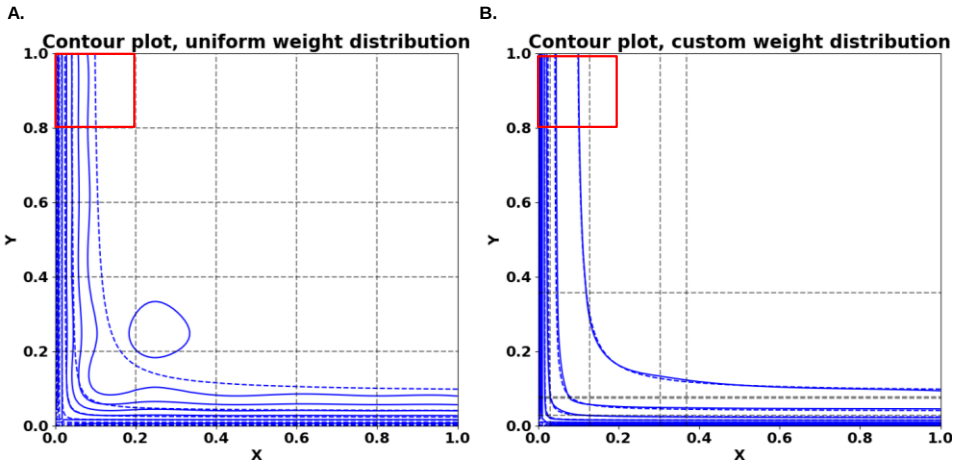

Figure 8: Contour plots showing the knots distribution (dotted grey lines), the dataset (dotted blue lines) and the spline approximation (blue lines). A. Using a uniform weight distribution. B. Using a custom weight distribution. Both plots are obtained after running the knots optimization algorithm.

The results of the optimization are shown in Figure 7B and Figure 8B. In that case, the knot optimization converges properly as the algorithm is able to allocate more knots to the steep region in order to properly fit it.

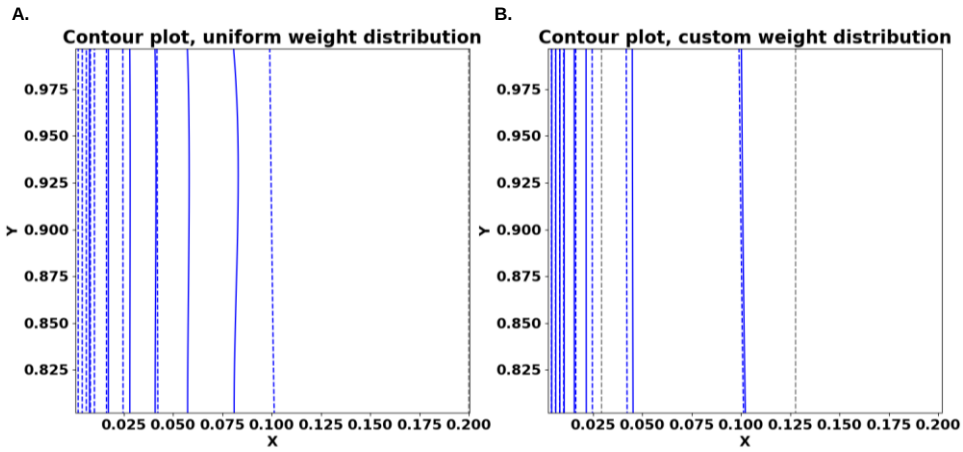

Figure 9: Detail of the contour plots shown in Figure 8. The area displayed corresponds to the red squares located on each plots.

Figure 9 shows the steep region in greater details. In Figure 9A we can see that the splines approximation does not capture the steep gradient as the contour lines do not match. On the other hand, with the custom weight distribution (Figure 9B), the match is much better.

3. RESULTING SPLINES DEFINITION

In this section, we discuss the precision of our spline formulation across the single phase region. First, we control relative errors to ensure that all are less than an error margin of 1%. Second, we explore the behavior of the partial derivatives. Finally, we compare our formulation to the IAPWS formulation in the vicinity of a thermodynamic boundary.

3.1. Error quantification

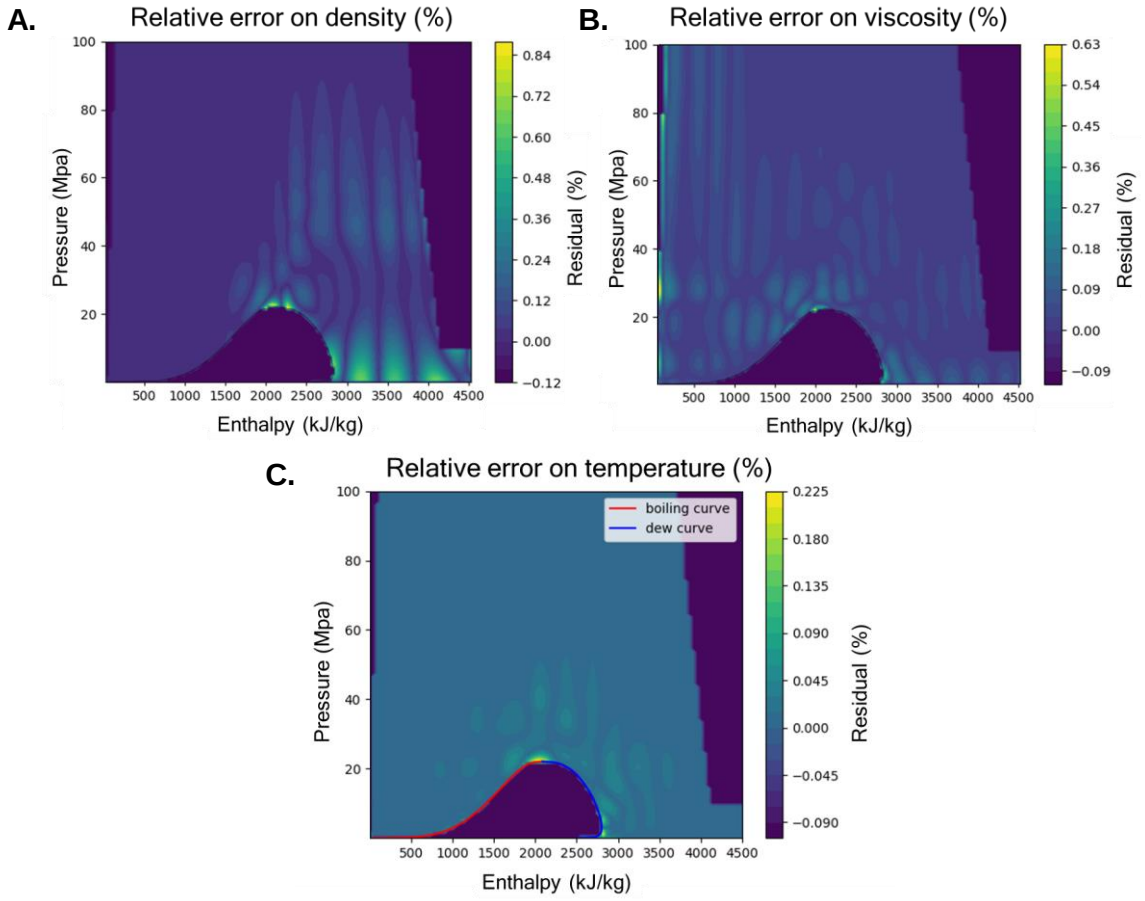

Figure 10: Contour plots showing the relative error between the dataset and our spline approximation for density (A), viscosity (B) and temperature (C). The error is not measured in the two-phase region, defined as the area under the boiling and dew curves denoted by red and blue lines, respectively, in the lower plot.

Figure 10 shows the relative error between our spline approximation and the IAPWS formulation, computed as $\varepsilon = 100 \times \text{abs}\left(\frac{(z_{spl} - z_{IAPWS})}{z_{IAPWS}}\right)$. The best fit temperature surface has a maximum error of 0.225% (Figure 10C). All three surfaces have relatively high errors around the critical point, which is expected as this region presents a highest degree of complexity. We can see in all three plots that the error has an oscillatory component. This phenomenon is the result of a lack of smoothness in the spline approximation, which leads to higher residuals between data points. However the amplitude of the oscillations is small enough to not constitute an issue. None of the spline approximations exceed an error of 0.9%.

3.2. Partial derivatives of fluid properties

Inspection of the first order derivatives is a reliable way to assess the smoothness of our spline approximation. A region that is not smooth enough will present local changes in the sign of its derivatives. Such behavior is unacceptable if the formulation is to be used in a numerical simulation software as it would create artificial local minima.

Appendix A shows the partial derivatives for all three fluid properties with respect to both pressure and enthalpy. The derivatives do not present any artificial changes in their sign which suggests that our spline approximations are sufficiently smooth. At low enthalpies, the partial derivative of density with respect to pressure shows some abnormal variation in the derivative. This behavior is linked to the oscillation component of the spline approximation. However, the amplitude of the phenomenon is small enough that it does not change the sign of the derivative. This issue is further illustrated in Figure 11, which displays the relative error between the partial derivatives obtained using a finite difference method on the IAPWS dataset and the one obtained using our splines-based formulation.

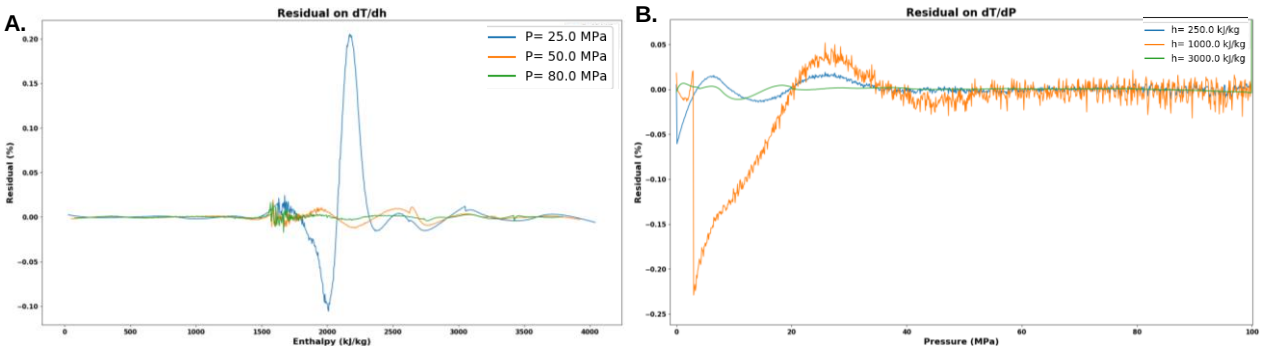

Figure 11: A. Residuals of the partial derivative of temperature with respect to enthalpy at different pressures. B. Residuals of the partial derivative of temperature with respect to pressure at different values of enthalpy.

The plotted residual has two components: a high frequency, low amplitude oscillation related to the finite difference, and a low frequency component due to the spline approximation. The amplitude of the second component is strongest in the vicinity of the critical point (P = 22 MPa, h = 2088 kJ kg^{-1}). This is expected as this region has the highest relative errors.

3.3. Continuity

We have elected to fit thermodynamic regions 1, 2, 3 and 5 with a single spline approximation to ensure continuity of the formulation across the region boundaries. Figure 12 shows a cross section of temperature with respect to enthalpy just above the critical point, crossing the boundaries between regions 1 and 3, and 3 and 2.

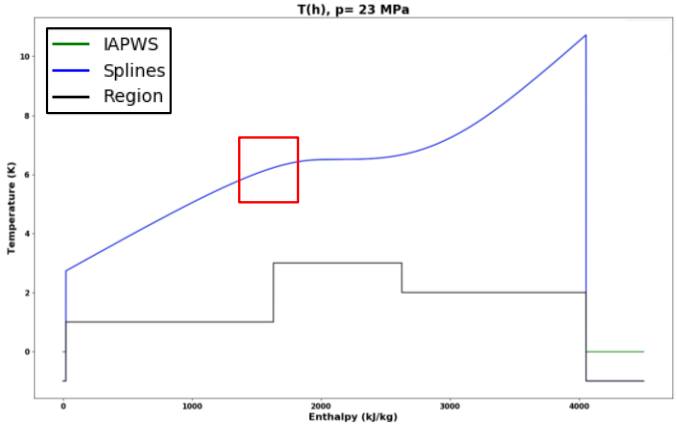

Figure 12: Temperature with respect to enthalpy for constant pressure (23 MPa) using the IAPWS formulation (green curve) and our splines formulation (blue). The black line shows the thermodynamic region along the profile. For scale purpose the temperature has been divided by 100. The red square is the location of the close up displayed in Figure 13.

The IAPWS formulation presents a slight discontinuity between the values of temperature on the boundary between region 1 and region 3, given on one side by the Gibbs equation and on the other by Helmholtz's (Figure 13). This discontinuity is relatively small but can cause convergence issues when crossing those boundaries during a flow simulation. Our spline approximation is smooth across the boundary.

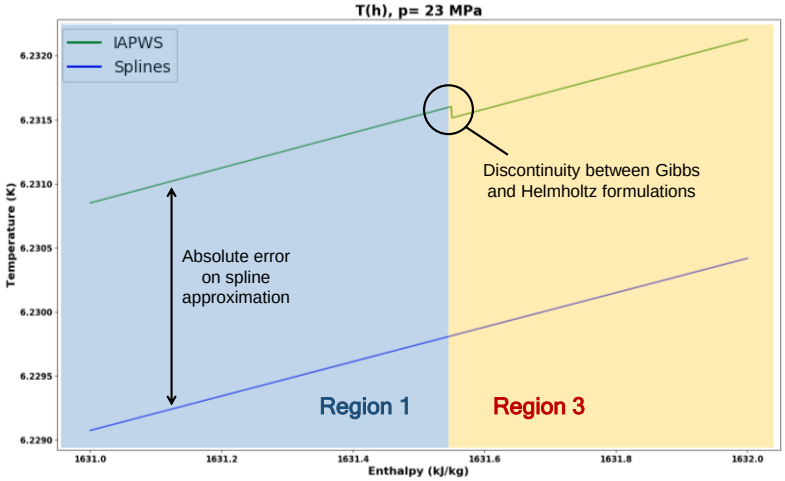

Figure 13: Close up of the temperature profile displayed in Figure 12 around the boundary between region 1 and 3. The blue line is obtained using the spline formulation while the green curve is obtained using the IAPWS formulation.

4. IMPLEMENTATION INTO A FLOW SIMULATION SOFTWARE

For testing purposes, we implemented our thermodynamic formulation into the geothermal flow simulator Waiwera (Croucher, 2018). Waiwera uses the finite volume method to compute multiphase flow and heat transfer of a fluid within a porous medium. The software solves for conservation of mass and energy with fluid velocities given by Darcy's law. The fluid can be pure water or a mixture of water with a gas (CO_2, air…). In the case of pure water, the software uses either the IAPWS or IFC-67 formulation to compute the thermodynamic properties. In order to carry our tests, we added an equation of state based on our splines. Then, we designed simple test cases to compare the results obtained by a conventional IAPWS water thermodynamic formulation with the ones obtained using our spline based formulation.

4.1. 2-cell model

4.1.1. Model description

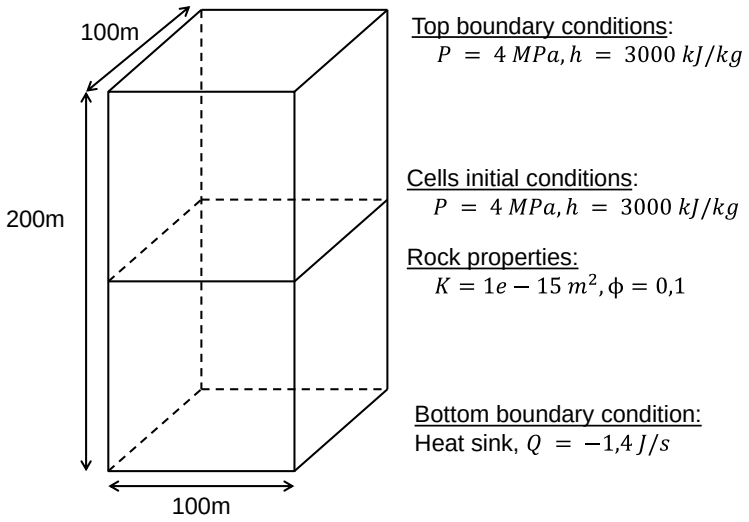

Figure 14: Schematic showing the layout of the two cell model as well as the boundary and initial conditions.

The first model has two cells (Figure 14). In the initial state, the water is in a vapor phase. A heat sink is applied at the base of the bottom cell. We expect a decrease in enthalpy at constant pressure. The heat flux is configured so that the fluid should transition from vapor to two phase to liquid state.

4.1.2. Results

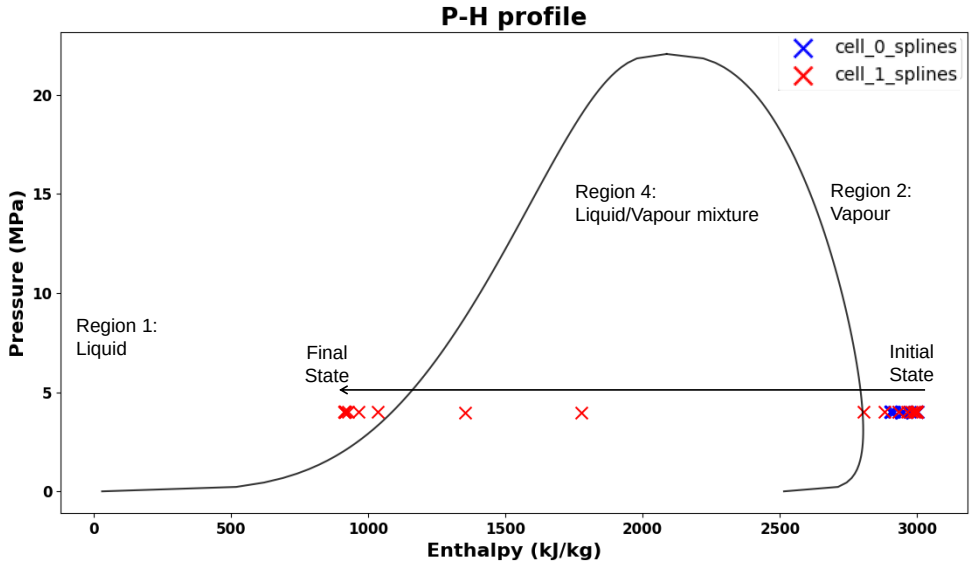

Figure 15: *P-H* profile displaying the thermodynamic path of the bottom cell (red crosses) and the top cell (blue crosses). The black curve represent the boundary between the single phase regions and the two phase region.

This model exhibits the expected behavior with enthalpy decreasing at constant pressure (Figure 15). At equilibrium, the bottom cell is in liquid state while the top cell remains pure vapor. Both formulations lead to the same variations in temperature and saturation (Figure 16).

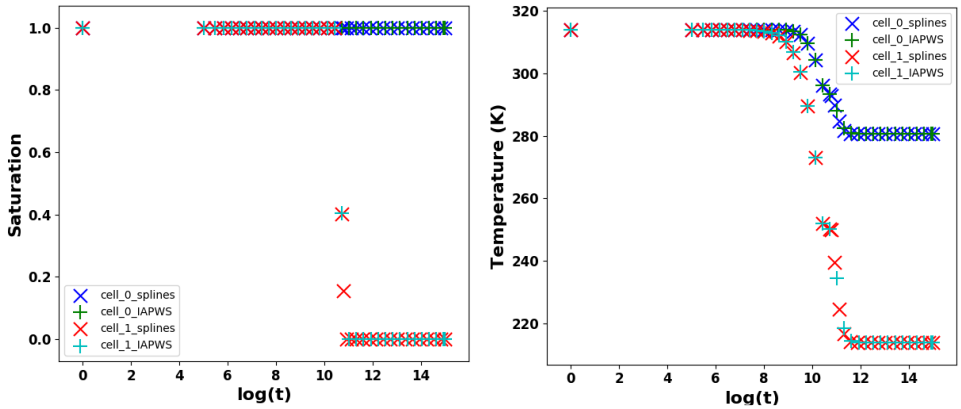

Figure 16: A. Saturation profile with respect to time using the IAPWS formulation and the splines formulation for the bottom cell (cell_1) and the top cell (cell_0). B. Temperature profile with respect to time using the IAPWS formulation and the splines for the bottom cell (cell_1) and the top cell (cell_0).

Both models converged without any problem since we got a linear correlation between the time and the length of the time step (Figure 17). The simulation using the splines formulation recorded a minor divergence from linearity at about 10^{11} seconds.

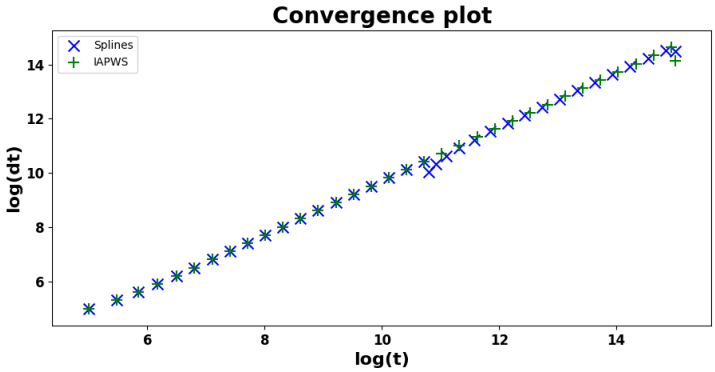

Figure 17: Convergence plot for the simulation using the IAPWS formulation (green plusses) and the splines formulation (blue crosses).

4.2. 2D production model

4.2.1. Model description

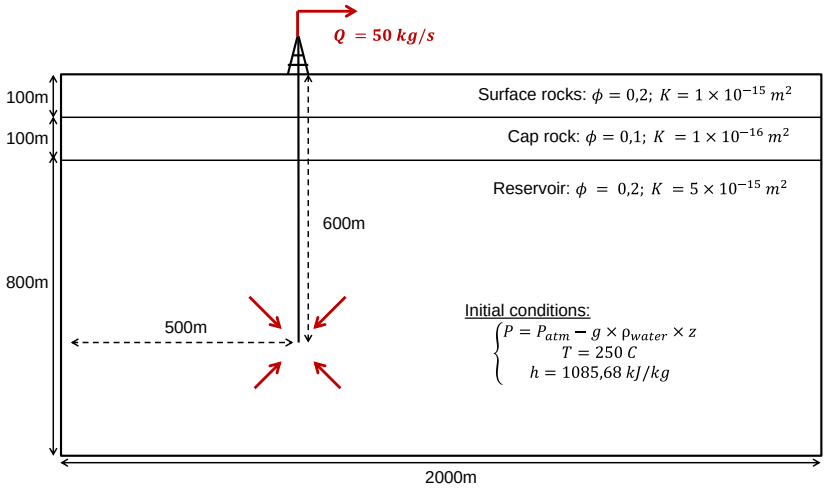

Figure 18: Schematic of the 2-D production model.

In this model (Figure 18), we consider an 800m-thick reservoir rock topped with a cap layer presenting a smaller permeability. The upper layer has intermediate rock properties. The domain is two kilometers wide and 1 kilometer deep. We introduce a production well with a feed zone located at a depth of 600m. The production rate is constant and equal to 50 kg/s. Initially, the model has a hydrostatic pressure gradient and an isotropic temperature and enthalpy. We divide the domain into a 40x40 grid. The dimension of the cells is 50x25 m. We simulate 50 years of production using both the IAPWS and splines thermodynamic formulations.

4.2.2. Results

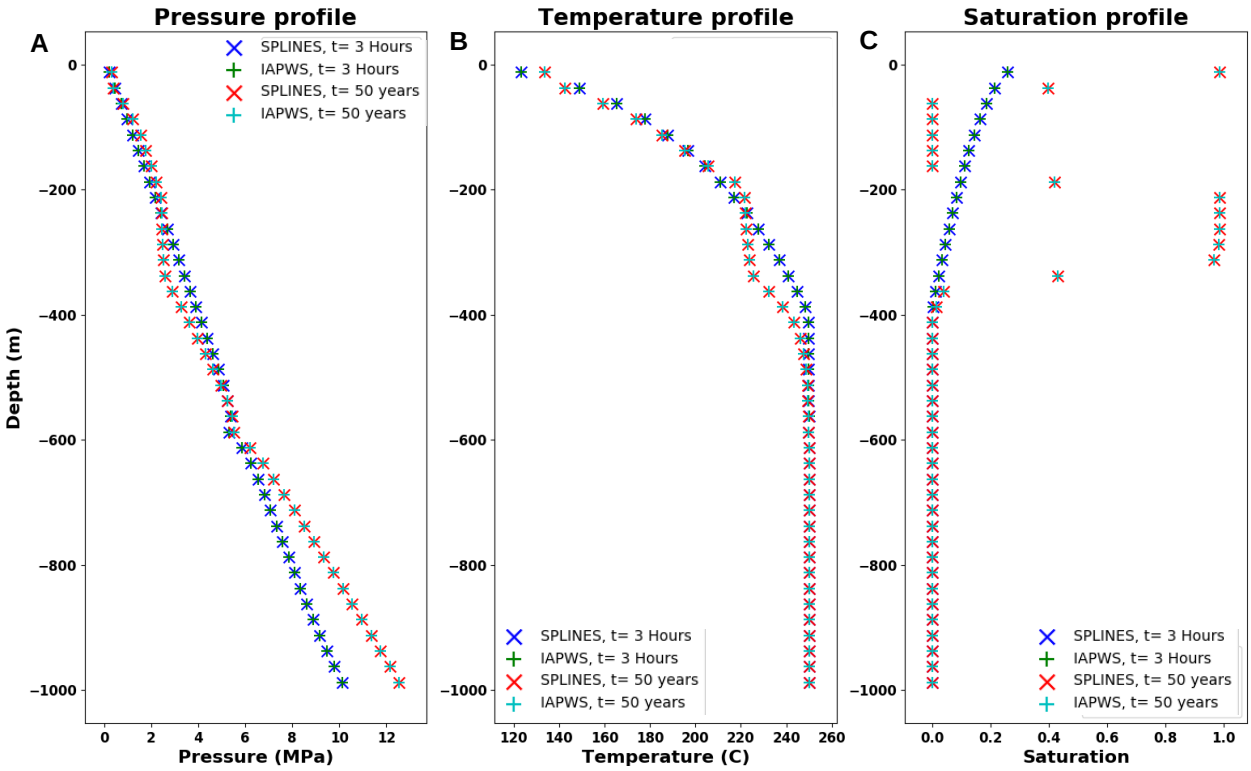

Figure 19: Vertical profiles taken along the well. A. Pressure. B. Temperature. C. Vapour saturation

Figure 19 shows vertical profiles of pressure, temperature and saturation in the reservoir. From these profiles) it is possible to distinguish the boundary between the reservoir and cap rock, at a depth of -200m, after 50 years of production. The mass flux coming out of the reservoir during production causes the pressure to drop in the upper part of the reservoir (from -200m to -600m). This pressure drop induces a decrease in temperature which drives the phase transition occurring in the upper part of the model. However, the pressure drop is also dependent on the permeability of the rock formation. The more permeable the rock is, the larger the pressure drop is. In the less permeable cap rock, the pressure drop is small enough to maintain the temperature of the fluid above the boiling point and no phase transition occurs.

5. CONCLUSION

We wanted to develop a smooth and easily differentiable formulation for the thermodynamic properties of water over the whole single phase domain. The bivariate splines approximation needed to smoothly capture all the complexity of our datasets. In order for our approximation to reach an acceptable quality, we had to optimize both the weight and knot distribution. In the formulation we presented, the largest relative error occurring is less than 1% and the partial derivatives are free from artifacts linked to the structure of the spline approximation. We have demonstrated that the new formulation is sufficient for calculations in a multi-phase geothermal flow simulator. However, the formulation could still be improved through further adjustment of the knot optimization parameters and weight distribution.

REFERENCES

Åberg, Marcus, Johan Windahl, Håkan Runvik, and Fredrik Magnusson. “Optimization-Friendly Thermodynamic Properties of Water and Steam,” 449–58, 2017. https://doi.org/10.3384/ecp17132449.

Torsten Schütze and Hubert Schwetlick. “Bivariate Free Knot Splines”, 2001.

The International Association for the Properties of Water and Steam. “Guideline on the Fast Calculation of Steam and Water Properties with the Spline-Based Table Look-Up Method (SBTL)”, 2015.

The International Association for the Properties of Water and Steam. “Revised Release on the IAPWS Industrial Formulation 1997 for the Thermodynamic Properties of Water and Steam”, 2007

Jain Rahul, Kannan M. Moudgalya, Peter Fritzson, and Adrian Pop. “Development of a Thermodynamic Engine in OpenModelica,” 89–99, 2017. https://doi.org/10.3384/ecp1713289.

International Association for the Properties of Water and Steam. “Revised Release on the IAPWS Formulation 1995 for the Thermodynamic Properties of Ordinary Water Substance for General and Scientific Use”, IAPWS R6-95(2016), 2018.

O’Sullivan, John, Mike O’Sullivan, and Adrian Croucher. “Improvements to the AUTOUGH2 Supercritical Simulator with Extension to the Air-Water Equation-of-State.” *Geotherm Resour Counc Trans* 40 (2016): 921–929.

Adrian Croucher, John O’Sullivan, Angus Yeh and Mike O’Sullivan. “Benchmarking and experiments with Waiwera, a new geothermal simulator”, 2018.

APPENDIX A: PARTIAL DERIVATIVES OF FLUID PROPERTIES

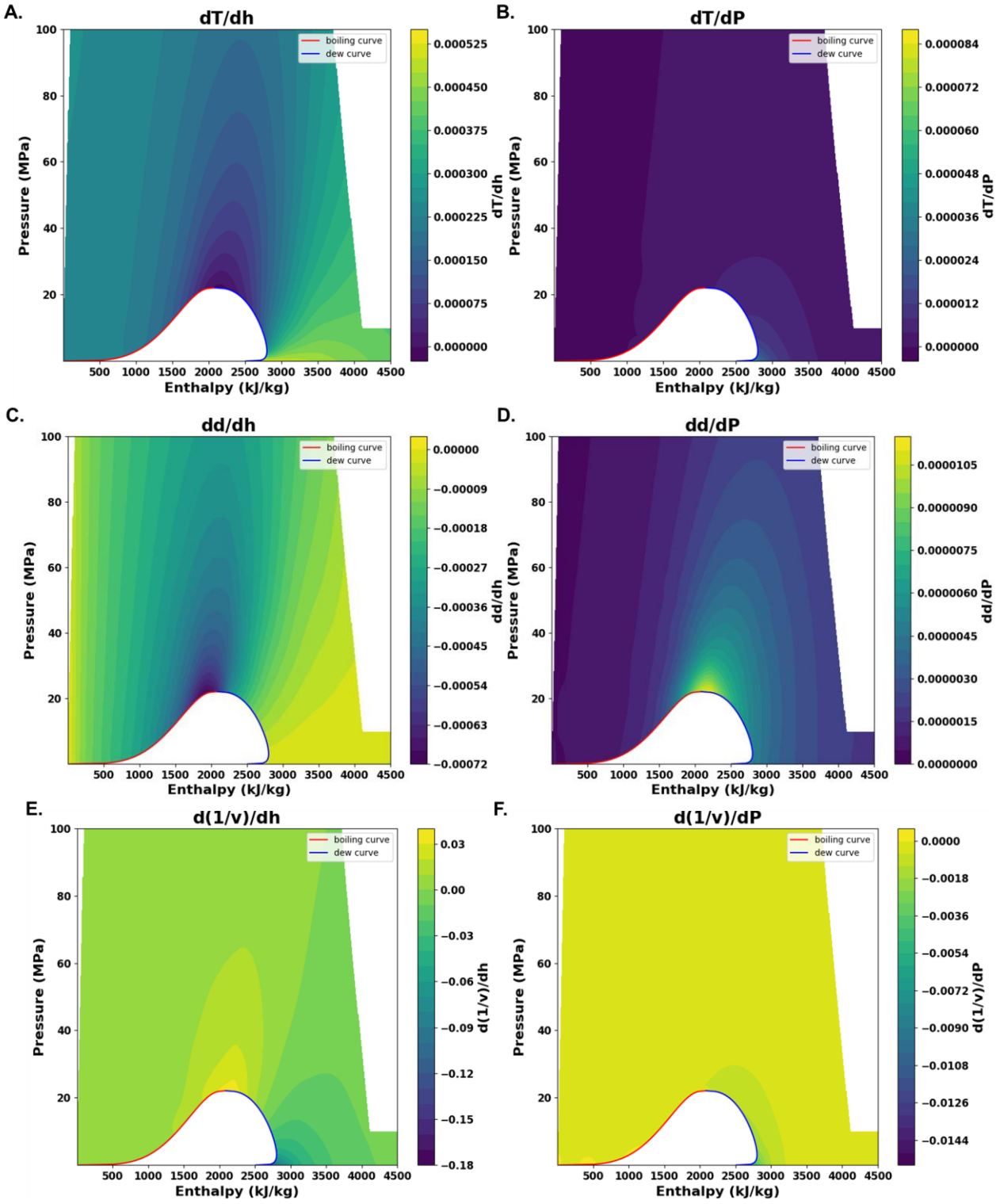

Figure 20: Contours plot of the partial derivatives. A. Temperature with respect to enthalpy. B. Temperature with respect to pressure. C. Density with respect to enthalpy. D. Density with respect to pressure. E. Viscosity with respect to enthalpy. F. Viscosity with respect to pressure.